Remote-controlled droplet chains-based electricity generators

Abstract

Harnessing ambient renewable mechanical energies for achieving carbon-neutrality generally demands the rational design of materials and architectures which are favorable for both energy collection and conversion simultaneously. However, the direct coupling of energy collection and conversion modules leads to many unwanted problems such as material wearing, spatial constraint for large-scale integration, and low energy conversion efficiency. Herein, we develop a remote-controlled energy harvesting strategy that cleverly harnesses the unique advantage of diffusive, long-range air flow within confined capillary channel, imparting to separate the energy collection unit, made of elastic cavity that directly transforms external mechanical motion to pneumatic motion, from the conversion units, made of encapsulated droplet chains that serve to translate their recurring motion within the capillary channel into electrical output. Particularly, distinct from single-drain electrode design for electricity generation from fresh droplets in the open space, we design two drain electrodes to collect and release electrostatically induced charges from recurring droplets in the confined channel, respectively, thereby eliminating the unwanted charge accumulation on recurring droplets and leading to efficient output performance. The integration of multiple electricity generation units with such a two-drain electrode architecture with a single energy collector improves the design resilience and relaxes the spatial limitation.

Introduction

Addressing energy and climate challenges requires the comprehensive exploitation of carbon-neutral energy sources[1-5]. Although abundant renewable and carbon-free energies are contained in our living surroundings, such as water waves[6-10], rain droplets[11-19], wind[20,21], and biomechanical motions[22,23], their intrinsic limitations of low frequency and irregularity impede the efficient translation of their energies into

electricity via the conventional electromagnetic-based approach[24]. As we enter the era of the Internet of Things, harnessing these omnipresent mechanical energies has become increasingly essential for the perspective of powering the worldwide distributed small electronics. To this end, various new techniques have been developed in recent years for harnessing these ambient mechanical energies, including triboelectric nanogenerators (TENGs)[25-29], piezoelectric generators (PEGs)[30,31], and droplet-based electricity generators (DEG)[18,32].

These emerging energy conversion techniques generally rely on the coupling in energy collection and the subsequent conversion, directly translating the external input into electricity through various mechanisms[33-41]. For example, the external impact on a TENG or a PEG device triggers the material deformation at the area underneath the impact, which leads to on-site electricity generation via electrostatic induction or piezoelectric effects. Similarly, for a DEG device with transistor-like architecture including source, drain, and gate terminals[42], the droplet impact induces the charge reformulation in the modules beneath the impact area, and thereby directly translating droplet kinetic energy into electricity (as shown in Fig. 1a). Although these techniques are all capable of converting small mechanical energies into electricity, their common weakness of the utility of on-site energy conversion strategies leads to several essential bottlenecks. On the one hand, the severe impact on the whole device would easily cause material wearing and devices' functional degradation. On the other hand, the coupled energy collection and conversion constructions impose significant challenges in achieving high space utilization for the large-scale integrated device and high energy harvesting efficiency, impeding the development of real applications.

Here we propose a remote-controlled droplet chains-based electricity generator (RC-DEG) by separating the coupled energy collection and electricity generation modules into different domains. An elastic cavity is utilized as an energy collector to convert the external mechanical motion into pneumatic

motion, which subsequently triggers the recurring movements of the encapsulated droplet chains in the slippery tubes located at the electricity generation domain. The separated energy collection and conversion strategy cleverly harnesses the unique advantage of diffusive, long-range air flow to eliminate the direct contact-induced material wearing, relax the spatial constraints for large-scale integration, and more importantly, endow the building of one energy collector with multiple electricity generation units for generating multiplied electricity output upon one trigger. Particularly, distinct from previous droplet electricity generation with single-drain electrode design limited to fresh droplets in the open space, we design two drain electrodes to efficiently collect and release electrostatically induced charges from recurring droplets in the confined channel, respectively, thereby eliminating the unwanted charge accumulation on recurring droplets and leading to considerable output performance. Our strategy skillfully expands the high-efficient droplet electricity generation from open-space to confined space and from the fresh droplets to recurring droplet, which are significant for broadening its range of applications. Additionally, with demonstrating the applications of RC-DEG for biomechanical energy harvesting, we anticipate that a broad range of technologies and applications towards renewable energies will be developed based on our proposed droplet chains-based electricity generation strategy.

Results and discussion

Fig. 1b shows the schematic drawing of our RC-DEG, in which the normally coupled energy collection and electricity generation modules are separated to allow for the energy harvesting in remote control manner. First, we choose the air as a unique transmission medium based on its diffusive and long-range features to allow for the translation of the external input into the moving motion of water through the entire RC-DEG by simply applying a mechanical force toward a rubber cavity (Fig. S1). To minimize the water viscous energy dissipation and maximize collective power generation, we choose the capillary

tube (FEP) with a very slippery property and high surface charge density as the core element of electricity generation module, which serves as both the dielectric layer and carrier for liquid transport. To further ensure efficient electricity generation, two-drain electrode design is used to efficiently collect and release electrostatically induced charges from recurring droplets in the confined channel, respectively. Besides imparting the preferred performances within one unit, separating the energy collection and conversion modules also endows the three-dimensional integration of multiple electricity generation units (Fig. S2), all of which can be actuated by a common input that resolves the spatial restriction encountered in conventional design.

The main body of the electricity generation module of our RC-DEG is constructed based on capillary tubes made of FEP material with a favored slipperiness, hydrophobicity, and strong charge affinity (each unit tube with a length of 20 cm and inner diameter of 4 mm). Two polished aluminum rings are placed at both sides of the unit tube, and a sheet electrode is wrapped half of the tube from outside (Fig. 1b). After the fabrication, we then fill water into half of the unit tube and use an air pipe to connect the rubber cavity and the FEP tubes so that the force-induced air pressure is endowed to be translated from the energy collection domain to the electricity generation domain to drive the movements of the droplets. The spacing between each droplet is ~ 10 cm (equaling half the length of the FEP tube unit), which can be tailored by controlling the volume of water injected into each unit. Each unit tube is carefully fabricated to connect with the adjacent unit with a U-type connecting tube to form the airflow channel for transmitting the air pressure changes. The schematic and the as-fabricated RC-DEG arrays are shown in Fig. 1b and 1c.

Fig. 1d shows that the measured voltage, current, and charge outputs from a single-unit RC-DEG are 370 V, 0.7 mA, and 65 nC, respectively. The instantaneous high peaks in voltage and current outputs appear when the moving water droplet contacts the two aluminum ring electrodes (Movie S1), in which water droplet behaves like a gate in analogy to a field-effect transistor (Table S1), whereas two ring

electrodes and the sheet electrode can be regarded as drains and source, respectively. Therefore, the contact between the water and the drain leads to the formation of a closed-loop circuit which allows for the flowing of charges between the source and the drain. Corresponding to the pressing and releasing of the rubber cavity, a single-unit RC-DEG is capable of lighting up 100 LEDs twice (Movie S2). Moreover, the RC-DEG device integrating eight electricity generation units can light up 800 LEDs by simply pressing on the cavity (Fig. 1c and Movie S3). The power generation can be further amplified by mounting up more units and leveraging on the precision manufacturing and mass production.

To demonstrate the advantage of our design, we also fabricate two control samples containing identical structure, size, and materials but different number of drain electrodes (Fig. 2a and S3). Under the same experimental conditions, the charge output from the RC-DEG featuring two- drain electrodes is four-fold higher than those of control samples. More pronouncedly, both the voltage and current outputs of the RC-DEG are around two orders of magnitude larger than those of the control devices (Fig. 2b-d), suggesting that the adoption of two-drain electrodes design is essential to the pronounced output.

To understand the underlying mechanism responsible for the enhanced output rendered by the two-drain electrode design, we further examine the mapping between transport dynamics of the water droplet and the corresponding charge transfer. Notably, the flow direction of charges between the source and drain is closely governed by the moving direction of water droplet (Fig. 3b and Movie S1). Moreover, this flow characteristic of the charge performs good stability during 3600 cycles (Fig. S4). Meanwhile, we also observe that the emergence of two electric current peaks originates from contacting of the gating water with the drain electrodes (Fig. 3c). Fundamentally, the two-drain design endows the RC-DEG with the capacity of efficiently collect and release the electrostatically induced charges, respectively, thereby eliminating the unwanted charge accumulation and leading to better output performance than two control groups (Fig. S5).

In detail, four characteristic time points (t_0, t_1, t_2, and t_3) and four corresponding stages (t_0-t_1, t_1-t_2, t_2-t_3, and t_3- t_0) are defined to describe the charge transfer process during one cycle of droplet movement (Fig. 3d). Among, t_0 denotes the initial time when the water droplet is at the left side of the unit and conductively connects with the drain-I. In the first stage (t_0-t_1), the water droplet starts to move to the right direction yet maintaining conductive connection with the drain-I when pressure balance inside the tube is broken by pressing the cavity located at the leftmost of the device. From the circuit perspective, a closed-loop circuit between the drain-I, source and the FEP is established. With the water droplet movement, electrostatically-induced positive charges on the source gradually transfer to the drain-I. The process terminates when the water droplet detaches from the left drain-I at the time t_1. Then, moving to the second stage (t_1-t_2), the charge transfer process stops because the loop circuit is open. When the water droplet connects with the right drain-II at t_2, the open-loop circuit is switched on again, accompanied by the quick transfer of positive charges from the source to drain-II and hence a high current peak. Meanwhile, the charge transfer process moves to the third stage (t_2-t_3). The charge transfer process terminates when the water droplet is oppositely driven to detach with the left drain-II quickly under negative pressure induced by the released cavity. This quick detachment results in the accumulation of electrostatically-induced charges in the water droplet. Next, an opposite high current peak is formed at t_3 when the water droplet connects with the drain-I again. In the final stage (t_3- t_0), the accumulated charges fully transfer from the connected drain-I to the source electrode. This process stops when the water droplet moves back to the original location. The recurring droplet also recovers its original status in electrical property. To furtherly understand the underlying mechanism of the whole charge transfer process, we develop a theoretical model based on the transport dynamics of the recurring droplet (Fig. S6) and the electrostatic induction (Supporting information note 1, Table S2, Fig. S7). The charge output obtained by the theoretical model has a good agreement with the experimental results (Fig. S8).

Understanding the basic charge transfer process enables us to investigate the parameter influencing the performance of the RC-DEG devices. Fig. 4a shows that the measured peak current output is reversely proportional to the load resistance, and the maximum current and the power is around 0.7 mA and 80 mW, respectively. Note that the electrical output can be enhanced further by increasing the unit length (Fig. S9). As shown in Fig. 4b, the charge, voltage, and current outputs of the RC-DEG become larger as we increase the unit length (Fig. S10). In addition to the unit length, we also determine the optimal driven frequency for energy generation (Fig. S11). Varying the driven frequency ranging from 0.25 Hz to1.5 Hz, we achieve the maximum performance of the RC-DEG at ~ 1 Hz probably owing to the best stability of surface charge and the water dynamics (Fig. 4c). Fig. 4d and Fig. S12 shows the time-dependent variation of the voltage for the RC-DEG connecting to capacitors of 4.7 μF, 10 μF, 22 μF, and 47 μF, in which a maximum voltage of 10.5 V can be obtained within 500 s charging (The left figure of Fig. 4d). We also quantitatively demonstrate the capacitor charging performance of the integrated RC-DEG (The right figure of Fig. 4d). A capacitor of 47 μF can be charged to 0.8V, 1.5 V, and 7.0V in 10 min by the RC-DEG containing 1, 2 and 10 units, respectively, at a frequency of 1Hz, exhibiting a linearly proportional relationship between the output voltage and the unit number. For practical applications, the synergy of the integration and indirect-control capability of our RC-DEG endows assembling of a large amount of the arrayed RC-DEG devices. This multi-unit integration strategy also has the capacity to broaden the output voltage bandwidth in parallel connection (Fig. S13).

The RC-DEG can also serve as a generic toolkit for energy harvesting in various application scenarios (Fig. 5a). During the COVID-19 outbreak, wearing face masks has been recommended as an important public measure for control and prevention of spread of SARS-CoV-2 variants. However, reducing the face mask leak and ensuring the continuous monitoring of mask status, especially for children, still present a great technological challenge. Here, we develop a self-powered mask wearing status monitoring system

based on our presented RC-DEG, which can be embed with the face mask and enables a high-efficient conversion of the gas pressure fluctuation energy generated by the respiration in the confined space between the face and the face mask (Fig. 5b). The monitoring system can generate synchronously a blink reminder on the liquid crystal display screen with the respiration, if the face mask is worn properly (Movie S4). On the contrary, the monitoring system will stop working due to the insufficient power supply when the face mask is worn improperly. Additionally, we also demonstrate the RC-DEG's energy harvesting capability in shoe energy harvesting (Fig. 5c). We assemble an integrated RC-DEG with a rubber cap as an energy collector and three electricity generation units into an insole to collect the walking energy. One single-stepping motion on the integrated RC-DEG can light up 63 LEDs in total twice (Fig. 5d): once for droplet moving first forwards and another for backwards, as shown in Movie S5.

Conclusion

In this work, we propose a generic energy harvesting strategy that indirectly converts the ambient mechanical energies into electricity with high efficiency by cleverly using the two-drain transistor-like architecture and separating energy collection and conversion into different modules. In contrast to previous direct electricity generation approaches, the proposed new RC-DEG circumvents many drawbacks including violent external impact, unwanted charge accumulation, the alignment between the energy source and the energy collection unit, and the spatial constraint for scalable integration. Particularly, the two-drain architecture efficiently collect and release electrostatically induced charges from recurring droplets in the confined channel, respectively, thereby eliminating the unwanted charge accumulation on recurring droplets and leading to current and voltage outputs two orders of magnitude higher than conventional designs. In coupling with the design of two-drain transistor-like architecture, separating the energy collection and conversion units endows the multiplexed electricity generation based on a single

energy collector. We envision that the droplet chains-based electricity generation strategy points a new direction for efficient ambient renewable energy harvesting for multi-scenario applications.

Methods

RC-DEG fabrication. The RC-DEG comprises an elastic cavity and an FEP (Fluorinated ethylene propylene) tube with an inner diameter of 4mm and an outer diameter of 5mm connected with the cavity. The FEP tube can be divided into several tube units with several tube units. For a typical unit with a length of 20 cm, we first cut the FEP tube into three sections with lengths of 5cm, 5cm and 10 cm, respectively. Then we connected these three tube elements via connectors, and at their junctions, we assembled in the Al rings with an inner diameter of 4mm as the drain electrode. The inner surfaces of the Al rings were polished to be very smooth and perfectly fitted the inner wall of the FEP tube, which enables the free movements of the water inside the tube. Copper tape (or copper-based cloth) with 10 cm length was wrapped outside the tube at one side of the unit as the source electrode. Electric wires were used to connect the drain electrodes and the source electrodes.

Microfluidic-based RC-DEG fabrication. A template of the microfluidic chip was first prepared by 3D printing technology. Then, a certain volume of mixed liquid of polydimethylsiloxane and curing agent (ration 10:1) was poured into the template and vacuumed for 1 h to remove internal gas. After curing for 30 minutes at 80°C, we peeled off the PDMS sample from the template and bonded it with a PDMS film. To construct the electrodes, ten metal needles were embedded in the microchannel as drain electrodes, five conductive Cu tapes of 2 mm×8 mm were assembled onto the PDMS film as external electrodes. Several electric wires were used to connect the drain electrodes and the source electrodes.

Characterization and electrical measurement. The water movement in the RC-DEG was recorded by a high-speed camera (Photron FASTCAM SA4) at a typical recording speed of 6000 fps. The voltage output

of RWT-TENG was measured using an oscilloscope (Rohde & Schwarz RTE1024) equipped with a high-impedance (10 MΩ) probe. The current and the transferred charges were measured using the oscilloscope coupled with a low-noise current preamplifier (Stanford Research System Model SR570) and a Faraday cup connected with a nanocoulomb meter (MONROE Model 284), respectively.

Data availability. The data that support the findings of this study are available from the corresponding authors on reasonable request.

Acknowledgements: We acknowledge the financial support from Research Grants Council of Hong Kong (No. C1006-20WF, No. 11213320), Tencent Foundation through the XPLORER PRIZE, Innovation and Technology Council (No. 9440248), National Natural Science Foundation of China (Grant Nos. 51975502 and 21621001), Science and Technology Planning Project of Guangdong Province (No. 2021A0505110002), Innovation Technology Fund(GHP/092/20GD), and the 111 Project (B17020).

Author contributions: Z.W. supervised the research. H.Z., H.W., Y.S. and Z.Y. conducted the experiment and data analysis. Z.Y., H.Z., Y.S. and W.X. built the model. All authors participated in the discussion of the experimental design. Z.W., H.Z., H.W. Z.Y. and S.W. wrote the paper. All authors commented on the paper.

Competing interests: The authors declare that they have no competing interests.

References

1 Chu, S. & Majumdar, A. Opportunities and challenges for a sustainable energy future. *Nature* **488**, 294-303 (2012).

2 Isaacs, J. D. & Schmitt, W. R. Ocean energy: forms and prospects. *Science* **207**, 265-273 (1980).

3 Schiermeier, Q. Solar and wind energy propel growth in US renewables. *Nature* (2017).

4 Stokstad, E. RENEWABLE ENERGY. A reboot for wave energy. *Science* **352**, 637-638 (2016).

5 Veers, P. *et al.* Grand challenges in the science of wind energy. *Science* **366** (2019).

6 Gu, H. *et al.* A bulk effect liquid-solid generator with 3D electrodes for wave energy harvesting. *Nano Energy* **87** (2021).

7 Liu, L., Shi, Q., Ho, J. S. & Lee, C. Study of thin film blue energy harvester based on triboelectric nanogenerator and seashore IoT applications. *Nano Energy* **66** (2019).

8 Wang, Z. L. New wave power. *nature* **542**, 159–160 (2017).

9 Wu, H., Wang, Z. & Zi, Y. Multi-Mode Water-Tube-Based Triboelectric Nanogenerator Designed for Low-Frequency Energy Harvesting with Ultrahigh Volumetric Charge Density. *Advanced Energy Materials* **11** (2021).

10 Zhu, G. *et al.* Harvesting water wave energy by asymmetric screening of electrostatic charges on a nanostructured hydrophobic thin-film surface. *ACS Nano* **8**, 6031-6037 (2014).

11 Jeon, S.-B., Kim, D., Yoon, G.-W., Yoon, J.-B. & Choi, Y.-K. Self-cleaning hybrid energy harvester to generate power from raindrop and sunlight. *Nano Energy* **12**, 636-645 (2015).

12 Jin, S. *et al.* Large-Area Direct Laser-Shock Imprinting of a 3D Biomimic Hierarchical Metal Surface for Triboelectric Nanogenerators. *Adv Mater* **30** (2018).

13 Lin, Z. H., Cheng, G., Lee, S., Pradel, K. C. & Wang, Z. L. Harvesting water drop energy by a sequential contact-electrification and electrostatic-induction process. *Adv Mater* **26**, 4690-4696 (2014).

14 Wu, H. *et al.* Charge Trapping-Based Electricity Generator (CTEG): An Ultrarobust and High Efficiency Nanogenerator for Energy Harvesting from Water Droplets. *Advanced Materials* **32** (2020).

15 Wu, H., Mendel, N., van den Ende, D., Zhou, G. & Mugele, F. Energy Harvesting from Drops Impacting onto Charged Surfaces. *Phys Rev Lett* **125**, 078301 (2020).

16 Xiong, J. *et al.* Wearable All-Fabric-Based Triboelectric Generator for Water Energy Harvesting. *Advanced Energy Materials* **7** (2017).

17 Xu, W. *et al.* SLIPS-TENG: robust triboelectric nanogenerator with optical and charge transparency using a slippery interface. *Natl Sci Rev* **6**, 540-550 (2019).

18 Xu, W. *et al.* A droplet-based electricity generator with high instantaneous power density. *Nature* **578**, 392-396 (2020).

19 Jin, Y. *et al.* Electrification of water: From basics to applications. *Droplet* **1**, 92-109 (2022).

20 Kaldellis, J. K. & Zafirakis, D. The wind energy (r)evolution: A short review of a long history. *Renewable Energy* **36**, 1887-1901 (2011).

21 Son, J.-Y. & Ma, K. Wind Energy Systems. *Proceedings of the IEEE* **105**, 2116-2131 (2017).

22 Bai, P. *et al.* Integrated multilayered triboelectric nanogenerator for harvesting biomechanical energy from human motions. *ACS Nano* **7**, 3713-3719 (2013).

23 Choi, Y.-M., Lee, M. & Jeon, Y. Wearable Biomechanical Energy Harvesting Technologies. *Energies* **10** (2017).

24 Zi, Y. *et al.* Harvesting Low-Frequency (<5 Hz) Irregular Mechanical Energy: A Possible Killer Application of Triboelectric Nanogenerator. *ACS Nano* **10**, 4797-4805 (2016).

25 Fan, F.-R., Tian, Z.-Q. & Lin Wang, Z. Flexible triboelectric generator. *Nano Energy* **1**, 328-334 (2012).

26 Wang, Z. L. On Maxwell's displacement current for energy and sensors: the origin of nanogenerators. *Materials Today* **20**, 74-82 (2017).

27 Fan, C., Wu, C., Wen, G., Wang, A. & Zhou, Q. Development of self-powered bubble velocity sensor for gas-liquid two-phase flow based on triboelectric nanogenerator. *Nanotechnology* **32**, 085503 (2021).

28 Munirathinam, K. *et al.* Flowing water-based tubular triboelectric nanogenerators for sustainable green energy harvesting. *Nano Energy* **102** (2022).

29 Zhang, X., Dong, Y., Xu, X., Qin, H. & Wang, D. A new strategy for tube leakage and blockage detection using bubble motion-based solid-liquid triboelectric sensor. *Science China Technological Sciences* **65**, 282-292 (2021).

30 Qin, Y., Wang, X. & Wang, Z. L. Microfibre-nanowire hybrid structure for energy scavenging. *Nature* **451**, 809-813 (2008).

31 Wang, Z. L. & Song, J. Piezoelectric nanogenerators based on zinc oxide nanowire arrays. *Science* **312**, 242-246 (2006).

32 Zhang, N. *et al.* A droplet-based electricity generator with ultrahigh instantaneous output and short

charging time. *Droplet* **1**, 56-64 (2022).

33 Tang, W. *et al.* Liquid-Metal Electrode for High-Performance Triboelectric Nanogenerator at an Instantaneous Energy Conversion Efficiency of 70.6%. *Advanced Functional Materials* **25**, 3718-3725 (2015).

34 Zhang, X., Zheng, Y., Wang, D. & Zhou, F. Solid-liquid triboelectrification in smart U-tube for multifunctional sensors. *Nano Energy* **40**, 95-106 (2017).

35 Wang, J. *et al.* Direct-Current Rotary-Tubular Triboelectric Nanogenerators Based on Liquid-Dielectrics Contact for Sustainable Energy Harvesting and Chemical Composition Analysis. *ACS Nano* **13**, 2587-2598 (2019).

36 Zhang, X. *et al.* Self-Powered Distributed Water Level Sensors Based on Liquid–Solid Triboelectric Nanogenerators for Ship Draft Detecting. *Advanced Functional Materials* **29** (2019).

37 Wu, H., Wang, S., Wang, Z. K. & Zi, Y. L. Achieving ultrahigh instantaneous power density of 10 MW/m(2) by leveraging the opposite-charge-enhanced transistor-like triboelectric nanogenerator (OCT-TENG). *Nature Communications* **12** (2021).

38 Zhang, N. *et al.* Boosting the output performance of volume effect electricity generator (VEEG) with water column. *Nano Energy* **73** (2020).

39 Yu, J., Ma, E. & Ma, T. Harvesting energy from low-frequency excitations through alternate contacts between water and two dielectric materials. *Sci Rep* **7**, 17145 (2017).

40 Yu, J., Ma, E. & Ma, T. Exponential energy harvesting through repetitive reconfigurations of a system of capacitors. *Communications Physics* **1** (2018).

41 Yu, J. & Ma, T. Triboelectricity-based self-charging droplet capacitor for harvesting low-level ambient energy. *Nano Energy* **74** (2020).

42 Xu, W. & Wang, Z. Fusion of Slippery Interfaces and Transistor-Inspired Architecture for Water Kinetic Energy Harvesting. *Joule* **4**, 2527-2531 (2020).

Figure captions

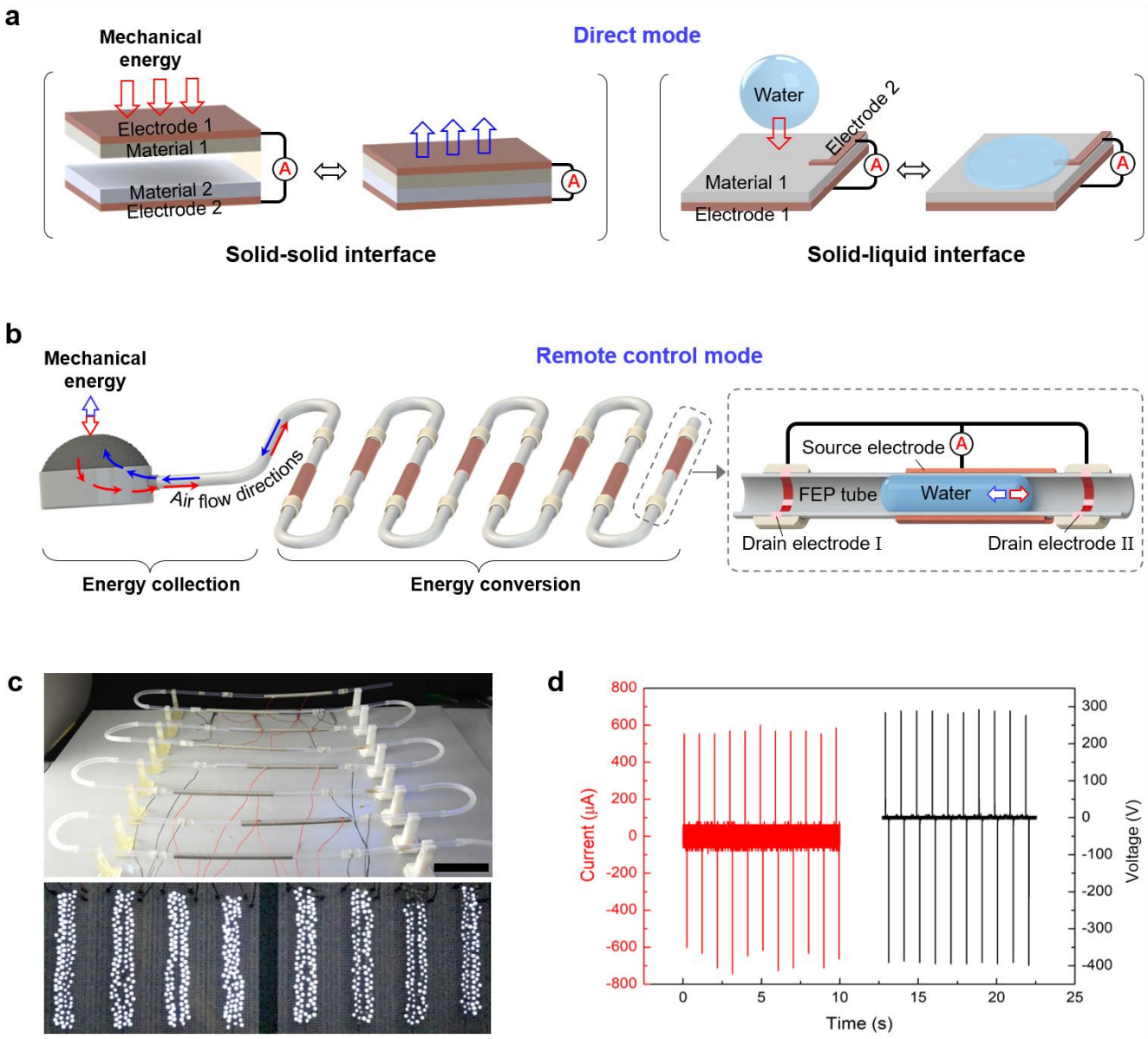

Fig. 1. Design of the RC-DEG. a. Schematic diagram of the conventional direct-mode electricity generators. **b.** Schematic diagram of the RC-DEG. Eight individual electricity generation units are connected in series and driven by an energy collector. Insert: schematic diagrams of an individual RC-DEG consisting of an FEP tube, water gate, two drain electrodes and a source electrode. **c.** 800 commercial LEDs are lighted up together powered by one RC-DEG device equipped with eight electricity generation units. Scale bar: 5 cm. **d.** The voltage and current outputs of a single-unit RC-DEG operating at the

frequency of 1.0 Hz.

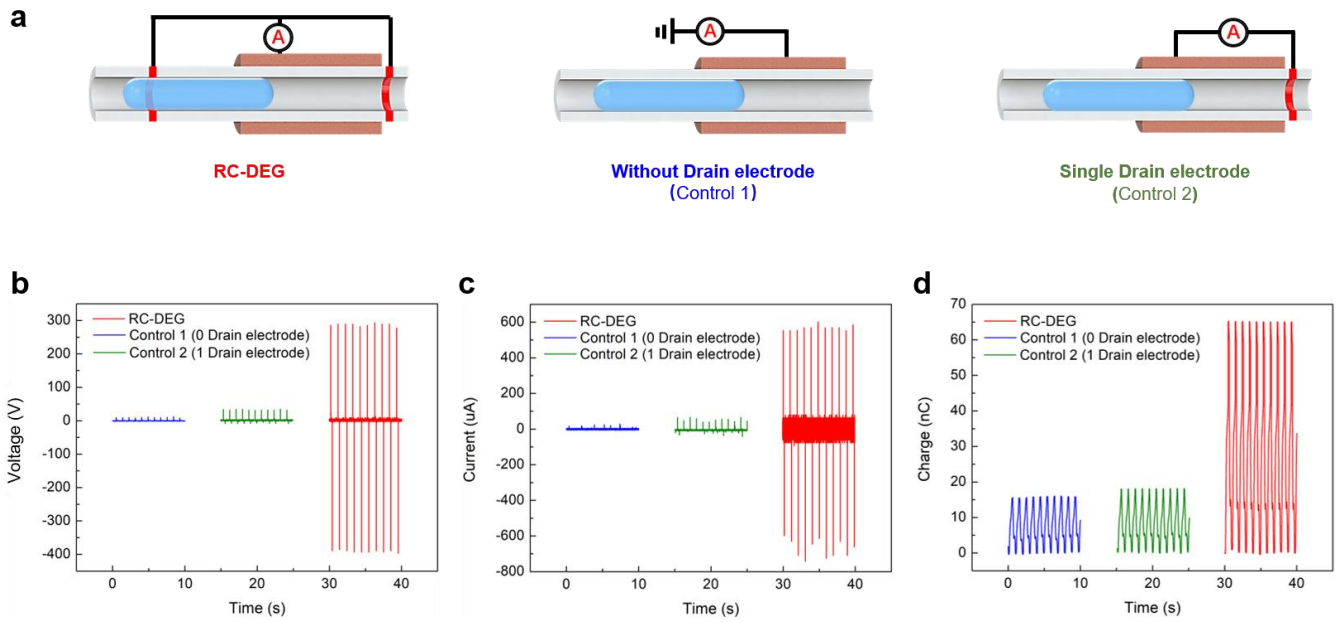

Fig. 2. The design of "drain" electrode of RC-DEG. a. Schematic of RC-DEG with two drain electrodes, the control devices with single electrode and without electrode. **b-d.** Comparison of the voltage, current and charge outputs from a single-unit RC-DEG and two control groups (operation frequency: 1.0 Hz).

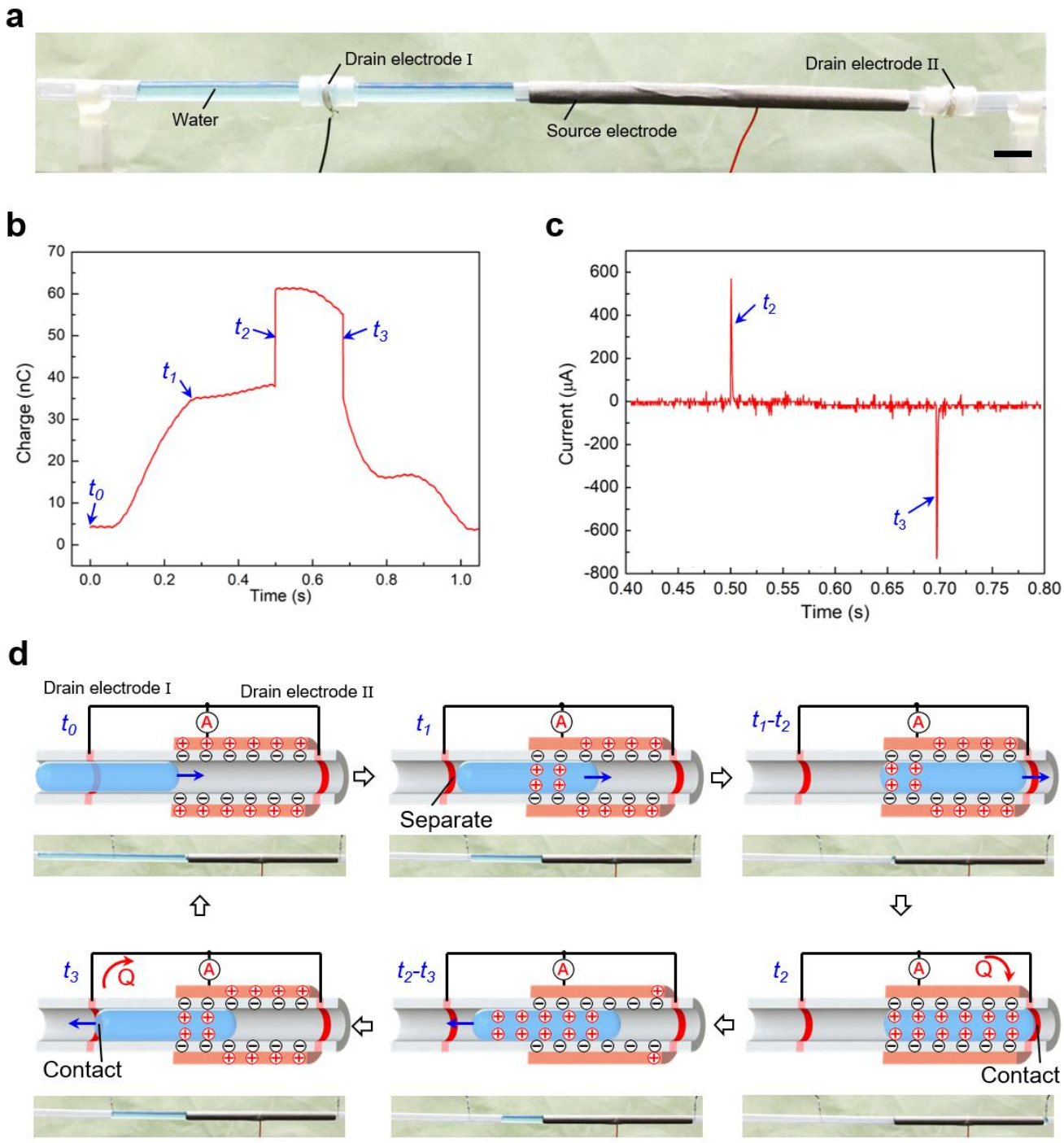

Fig. 3. Working mechanism of the RC-DEG. a. The optical photo of an individual RC-DEG. Scale bar: 1 cm. **b.** Time-dependent variation of the transferred charge between the source electrode and two drain electrodes during one cycle, indicating that the charge transfer has superior reversibility. **c.** Time-resolved

current variation corresponding to the charge transfer. **d.** Schematic drawing of RC-DEG working mechanism. Four stages (t_0-t_1, t_1-t_2, t_2-t_3, and t_3- t_0) segmented by four characteristic time points (t_0, t_1, t_2, and t_3) are defined to describe the charge transfer process during one cycle movement of the water droplet. In the first stage (t_0-t_1), the charge transfer process starts from the initial time t_0, when the water droplet is at the left side of the unit and connects with the drain-I, and terminates at the time t_1 when the water droplet detaches from the drain-I. The electrostatically-induced positive charges on the source gradually transfer to the drain with the droplet movement through an established closed-loop circuit between the drain electrode I, source and the FEP. Then, moving to the second stage (t_1-t_2), the charge transfer process stops because the loop circuit is open. When the water droplet connects with the right drain-II at t_2, the loop circuit is closed again, which accompanies by the quick transfer of electrostatically induced charges. Meanwhile, the charge transfer process moves to the third stage (t_2-t_3). The charge transfer process terminates at the time when the water droplet to detach from the right drain-II, resulting in charge accumulation in the droplet, and recovers at the time t_3 when the droplet moves to the left direction and contact with the drain-I. In the final stage (t_3-t_0), the accumulated charges gradually transfer from the drain-I to the source electrode and will stop when the water droplet moves back to the original location. The pictures below each schematic are optical photographs at the corresponding moment.

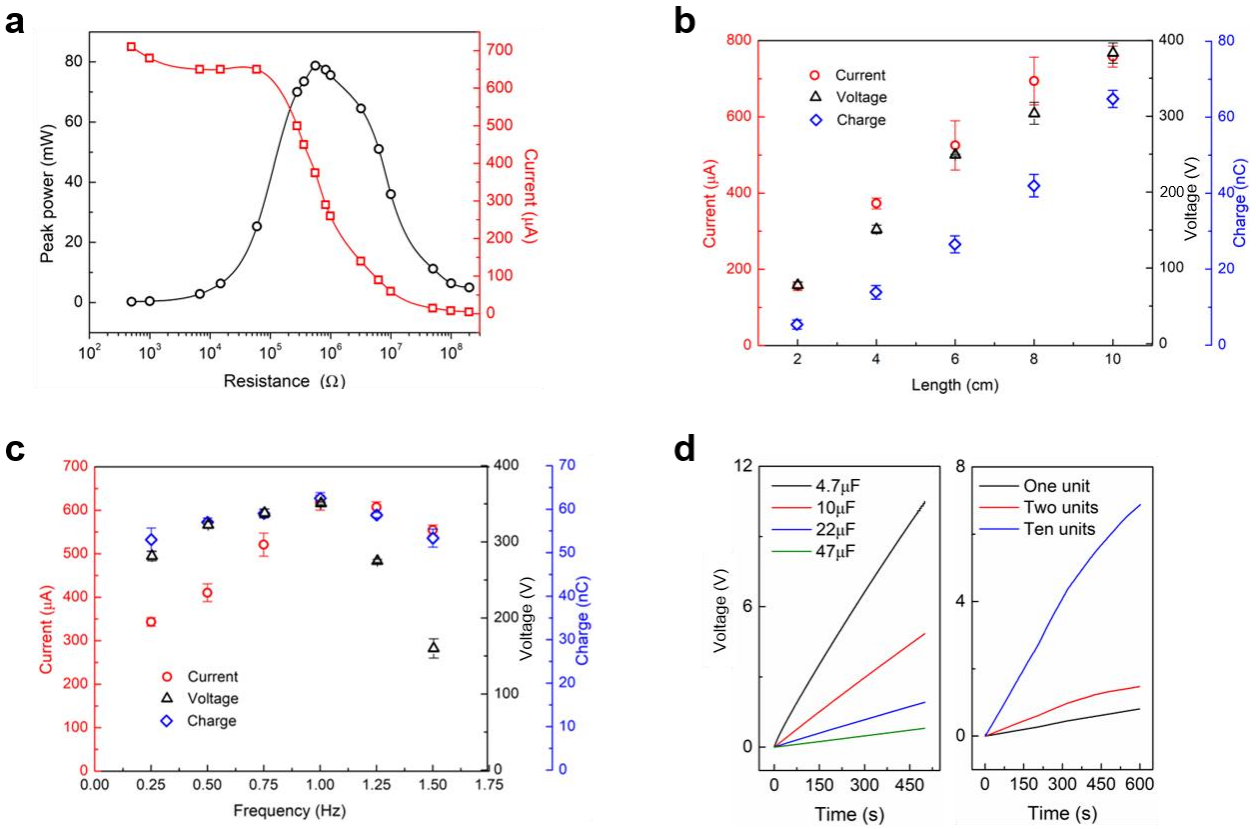

Fig. 4. Performance of the RC-DEG. a. Generated current and power of the single-unit RC-DEG depending on load resistance. The voltage, current and charge outputs of the single-unit RC-DEGs with **b.** varying the unit lengths and **c.** the operation frequency. **d.** Capacitor charging performance of single-unit RC-DEG aiming at the different capacitors with distinctive capacity and the RC-DEG with one, two and ten electricity generation units.

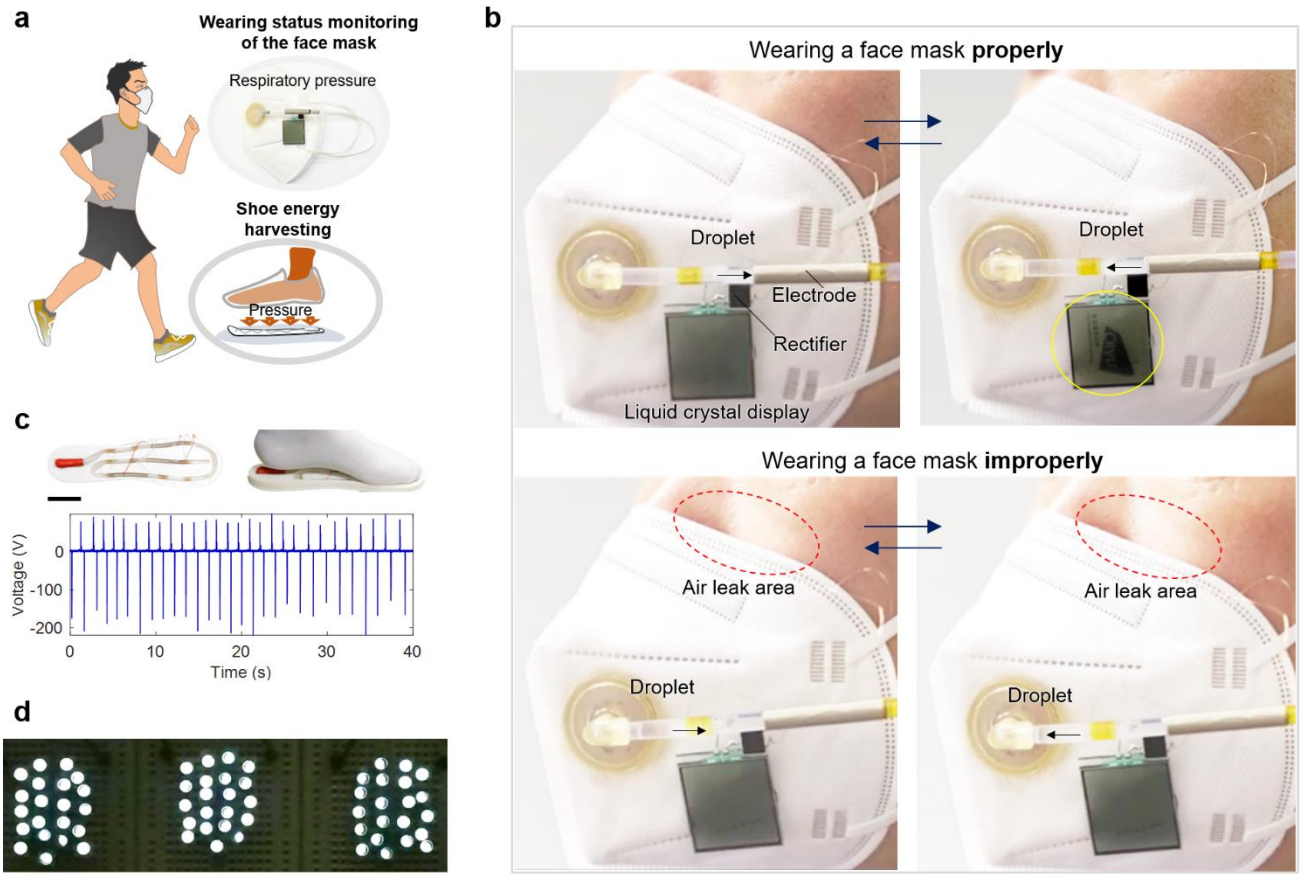

Fig. 5. Applications of the RC-DEG. a. The schematic diagram of the potential application scenarios of our RC-DEG. **b**. The status that a person wears a face mask properly and improperly. **c**. A wearable shoe's sole RC-DEG and the output voltage performance, Scale bar: 5 cm. **d**. Simultaneously lighting up 63 LEDs by using this wearable shoe's sole RC-DEG.